Meteorol Atmos Phys 84, 115–135 (2003)
DOI 10.1007/s00703-002-0578-2

Meteorology and Atmospheric Physics
Printed in Austria

[1] Geophysical Institute, University of Alaska Fairbanks, Fairbanks, AK, USA
[2] Staatliche Umweltbetriebsgesellschaft, Brandis, Germany
[3] Universität Halle-Wittenberg, Institut für Agrarökonomie und Agrarraumgestaltung, Halle/Saale, Germany

Long-term investigations on the water budget quantities predicted by the hydro-thermodynamic soil vegetation scheme (HTSVS) – Part I: Description of the model and impact of long-wave radiation, roots, snow, and soil frost

N. Mölders[1], **U. Haferkorn**[2], **J. Döring**[3], and **G. Kramm**[1]

With 10 Figures

Received October 8, 2001; revised February 15, 2002; accepted September 20, 2002
Published online: April 10, 2003

Summary

An earlier version of HTSVS was further developed to numerically investigate the long-term evolution of water budget elements (water supply to the atmosphere, ground water recharge, change in storage) in climate studies. In doing so, parameterizations of root effects, infiltration, soil frost, and snow insulation were included into HTSVS to predict these water budget elements for a period of 2050 days continuously covered by routine data of a lysimeter and a climate station. The results of simulations without and with inclusion of the new parameterizations as well as various sensitivity studies indicate that the insulating effect of a snow-pack, soil water freezing as well as the Dufour- and Ludwig-Soret-effects play a notable role on the long-term water budget and soil temperature evolution. Including frost effects yields improved soil temperature predictions. Snow density and, hence, snow depth play a key role for the prediction of soil temperature, freezing and the water supply to the atmosphere, but hardly affect deep soil water fluxes like recharge in the long-term sum. The results also show that the kind of vertical root distribution can be important for predicting water budgets. Based on these results we conclude that land surface models considered for long-term integration purposes require parameterizations of soil frost, snow and water uptake by roots to appropriately catch the broad cycle of soil water budget elements.

1. Introduction

Studies on water availability under recent and altered climate conditions require sophisticated climate models because recharge of ground water and soil moisture are processes that cannot be ignored on the long-term scale of the climate system. In areas of flat water tables, for instance, the consideration of groundwater re- and discharge is of great importance for predicting water availability because the water table will rise during long-lasting precipitation episodes, and it will sink or even uncouple from soil moisture during long-lasting drought episodes. Evidently, during droughts the lowered ground water table may contribute to their durations since evaporation from soil and transpiration by plants (summarized as evapotranspiration) and, hence, recycling of previous precipitation, are strongly reduced. On the contrary, long-lasting extreme precipitation events may trigger their persistence by recycling of previous precipitation because a high water table guarantees enough water available for evapotranspiration.

In high and mid-latitudes during winter as well as in high mountainous regions, soils are regularly frozen. Freeze-thaw cycles influence the thermal and hydrological properties of the soil because phase transition processes are accompanied by the release of latent heat and consumption of energy. Thermal conductivity of ice is about four times higher than that of water. Since frost reduces the mobility of soil-water, capillary action, infiltration, and percolation are rather inefficient. The low air temperatures, and, hence, the low saturation pressure of water vapor as well as the frequently stable stratification of the atmospheric surface layer (ASL) lead to less evaporation. In winter, transpiration plays a minor role because deciduous forests have already lost their leaves and even the stomatal conductivity values of coniferous forests are low during frost events compared to those observable during moderate weather conditions. Thus, moisture will be stored in frozen soils and may enhance spring peak flood events (Cherkauer and Lettenmaier, 1999).

Accumulated snow delays water input into the land phase of the water cycle (e.g., Dingman, 1994) and insulates the soil allowing only little heat exchange between the soil and atmosphere. Snow and snowmelt further affect the energy budget due to the change, for instance, (1) in albedo from 0.1 of a dark soil to 0.8 of fresh snow (e.g., Oke, 1978; Robinson et al, 1992), and (2) in emissivity from 0.95 of dark soil to 0.82 or so of old snow (e.g., Pielke, 1984). Exposed soil surfaces within partly broken snow coverage lead to substantial sensible heat fluxes, convection, and enhanced vertical mixing in the ASL. The strong spatial contrast in the energy budget of snow-covered and snow-free areas may generate a significant advection of heat and moisture similar to that usually accompanied by sea or vegetation breezes (Baker et al, 1999).

For all these reasons it is indispensable to establish the feedback mechanisms between the land and atmospheric part of the water cycle in climate modeling. Thus, any climate model requires a land surface model (LSM) that describes (1) the exchange of momentum, heat, and moisture at the *vegetation-soil-atmosphere* interface under special consideration of the heterogeneity on the micro-scale, (2) the insulating effects and retarded infiltration due to snow, (3) the heat conduction and water diffusion within the soil as well as the cross-effects (Ludwig-Soret-effect and Dufour-effect) generally generated by soil moisture and temperature gradients as postulated by the linear thermodynamics of irreversible processes, (4) soil freezing and thawing, (5) water uptake by plants, and (6) the variable ground water depth responding to the previous meteorological conditions. The hydrothermodynamic soil-vegetation-scheme (HTSVS; Kramm, 1995; Kramm et al, 1996; Mölders, 1999; 2000) that already fulfilled the requirements listed under points (1), and (3) has been further-developed for application in climate modeling by including a parameterization of infiltration, soil water extraction by roots, diagnostic approaches for soil frost and thawing, and consideration of the insulating effects and melting of snow.

The aim of this study is to evaluate the influence of soil frost, snow, and root water uptake on the long-term water budget quantities and soil temperature. In so doing, the stand-alone version of HTSVS is driven by meteorological data routinely observed at Brandis (51.32° N, 12.62° E, 133 m above sea level, south-east of Leipzig, Saxony).

2. Model description

To calculate the water supply to the atmosphere, two cases have to be distinguished: (1) the evapotranspiration by the vegetation-soil-system that has to be considered for snow-free conditions, and (2) the sublimation from snow that is semi-transparent to short-wave radiation.

2.1 Biosphere-atmosphere interaction

2.1.1 Resistance approaches

In HTSVS, vegetation is represented by a single layer. The exchange of energy and matter between the vegetation and atmosphere is parameterized in accord with the resistance networks shown, for example, in Kramm et al (1996). A mixture-approach analogous to Deardorff (1978) describes the heterogeneity of the vegetation-soil system on micro-scale, i.e., the effects of bare and plant-covered soil are linearly weighted by the shielding factor σ_f ($0 \leq \sigma_f \leq 1$) associated with the degree to which foliage prevents short-wave radiation from reaching the ground. Thus, the

governing flux equations for sensible heat, H, and water vapor, E, at the surfaces of foliage (index f) and soil (index g) read (e.g., Kramm et al, 1996)

$$H_f = -\sigma_f c_p \rho_a \left\{ \frac{1}{r_{mt,f}} (\Theta_\delta - T_f) - \frac{1}{r_{mt,fg}} (T_f - T_g) \right\}, \tag{1}$$

$$E_f = -\sigma_f \rho_a \left\{ \frac{1}{r_{mt,f}} (q_\delta - q_f) - \frac{1}{r_{mt,fg}} (q_f - q_g) \right\}, \tag{2}$$

$$H_g = -c_p \rho_a \left\{ \frac{1-\sigma_f}{r_{mt,g}} (\Theta_\delta - T_g) + \frac{\sigma_f}{r_{mt,fg}} (T_f - T_g) \right\}, \tag{3}$$

$$E_g = -\rho_a \left\{ \frac{1-\sigma_f}{r_{mt,g}} (q_\delta - q_g) + \frac{\sigma_f}{r_{mt,fg}} (q_f - q_g) \right\}, \tag{4}$$

where Θ_δ and q_δ are the values of potential temperature and specific humidity at the height δ close above the foliage. The surface temperature and specific humidity of foliage and soil are denoted as T_f, q_f, T_g and q_g, respectively. Furthermore, $r_{mt,f}$, $r_{mt,g}$, and $r_{mt,fg}$ are the resistances of the molecular-turbulent layer close to the surfaces of foliage and soil as well as the molecular-turbulent environment between the foliage and soil surface (index fg) against the transfer of heat and matter (e.g., Kramm et al, 1996). Moreover, ρ_a and c_p are the density and specific heat at constant pressure of air. As described by Kramm (1995), and Mölders (1999), the quantities Θ_δ, q_δ, and q_f can be derived by using Kirchhoff's law of electrostatics, where the eddy fluxes of sensible heat, H_t, and water vapor, E_t,

$$\begin{Bmatrix} H_t \\ E_t \end{Bmatrix} = -\frac{\rho_a}{r_t} \begin{Bmatrix} c_p(\Theta_R - \Theta_\delta) \\ q_R - q_\delta \end{Bmatrix}, \tag{5}$$

across the turbulent region of the ASL between δ and the reference height z_R, at which the meteorological measurements were performed, are considered. One obtains

$$\Theta_\delta = \frac{r_{mt,H} r_t}{r_{mt,H} + r_t} \left\{ \frac{1-\sigma_f}{r_{mt,g}} T_g + \frac{\sigma_f}{r_{mt,f}} T_f + \frac{\Theta_R}{r_t} \right\}, \tag{6}$$

$$q_f = \frac{1}{\frac{1}{r_{st}} + \frac{1}{r_{mt,fg}} + \frac{1}{r_{mt,f}}} \left\{ \frac{q_i}{r_{st}} + \frac{q_g}{r_{mt,fg}} + \frac{q_\delta}{r_{mt,f}} \right\}, \tag{7}$$

$$q_\delta = \frac{r_{mt,E} r_t}{r_{mt,E} + r_t} \left\{ \left\{ \frac{1-\sigma_f}{r_{mt,g}} + \frac{\frac{\sigma_f}{r_{mt,fg}}}{\left(\frac{1}{r_{st}} + \frac{1}{r_{mt,fg}} + \frac{1}{r_{mt,f}}\right) r_{mt,f}} \right\} q_g + \frac{\frac{\sigma_f}{r_{st}}}{\left(\frac{1}{r_{st}} + \frac{1}{r_{mt,fg}} + \frac{1}{r_{mt,f}}\right) r_{mt,f}} q_i + \frac{q_R}{r_t} \right\}. \tag{8}$$

Here, Θ_R and q_R are the potential temperature and specific humidity at z_R, $q_i = q_i(T_f)$ is the specific humidity within the stomata cavities that are assumed to be in saturated state, and

$$r_t = \frac{1}{u_* \kappa} \left(\ln \frac{z_R - d_0}{\delta - d_0} - \Psi_h(\zeta_R, \zeta_\delta) \right) \tag{9}$$

is the resistance of that turbulent region against the transfer of heat and matter. The quantities u_*, $\kappa = 0.40$, and $\zeta = (z - d_0)/L$ are the friction velocity, the von Kármán constant, and the Obukhov number, respectively, where L is the Obukhov stability length, d_0 is the zero-plane displacement, and z stands for both z_R and δ. Obviously, the turbulent resistance, r_t, depends on the thermal stratification of the turbulent part of the ASL characterized by Paulson's (1970) nondimensional integral stability function for heat and matter, $\Psi_h(\zeta_R, \zeta_\delta)$, in the version of Kramm (1989). The quantities $r_{mt,H}$ and $r_{mt,E}$ are defined by

$$\frac{1}{r_{mt,H}} = \frac{1-\sigma_f}{r_{mt,g}} + \frac{\sigma_f}{r_{mt,f}}, \tag{10}$$

$$\frac{1}{r_{mt,E}} = \frac{1-\sigma_f}{r_{mt,g}} + \frac{\left(\frac{1}{r_{st}} + \frac{1}{r_{mt,fg}}\right)\sigma_f}{\left(\frac{1}{r_{st}} + \frac{1}{r_{mt,fg}} + \frac{1}{r_{mt,f}}\right) r_{mt,f}}. \tag{11}$$

Transpiration of water by plants via stomata is described by Jarvis's (1976) approach for the bulk-stomatal resistance re-arranged to (e.g., Sellers et al, 1986; Hicks et al, 1987; Dingman, 1994)

$$r_{st} = \frac{r_{st,min}}{g_R(PAR) g_\delta(\delta_q) g_T(T_f) g_\eta(\Delta\eta) g_{CO_2}(CO_2)}. \tag{12}$$

Here, $r_{st,min}$ is the plant-specific minimum stomatal resistance (see Table 1). The sensitivity of bulk-stomatal resistance to photosynthetic active radiation, PAR, specific humidity deficit between leaf and ambient air, $\delta_q = q(T_f) - q_\delta$, leaf

Table 1. Plant specific parameters as used in the study. Here, Ψ_c, m, ρ_r, a (ranges from 0 to 2), R_r, $r_{st,min}$, b_{st}, T_{min}, T_{max}, T_{opt}, α_f, and ε_f are the soil water potential at which the production of cytokinis by roots is sufficiently reduced to close stomata, the fine root (oven-dry) bio-mass, the average volumetric density of roots (oven-dry), the partitioning of roots between the upper and lower root zone, the mean root radius, the minimum stomatal resistance, a parameter used to calculate stomatal resistance, the temperatures at which stomata close, the temperature at which $r_{st,min}$ reaches its minimum, the albedo and emissivity of foliage, respectively. Parameters are taken from Jackson et al (1996), Wilson et al (1986), and Kramm (1995)

Vegetation	Ψ_c m	m kg/m^2	ρ_r kg/m^3	a -.-	R_r 10^{-4} m	$r_{st,min}$ s/m	b_{st} -.-	T_{min} °C	T_{max} °C	T_{opt} °C	α_f -.-	ε_f -.-
Winter barley	−143	0.18	500	0.6	2.51	100	25	−1	35	20	0.21	0.95
Green fallow	−102	0.7	500	0.9	0.93	50	20	5	42	9	0.26	0.97
Red clover	−92	0.6	500	0.6	0.93	50	20	5	45	9	0.21	0.95
Potatoes	−92	0.1	500	1.5	2.51	110	40	5	42	23	0.21	0.95
Summer wheat	−102	0.164	160	1.3	5.10	100	25	5	40	24	0.21	0.95

temperature, T_f, soil moisture deficit, $\Delta\eta$, and the volumetric CO_2 concentration, $[CO_2]$, is considered by correction functions that are ranging from 0 to 1 (Jarvis, 1976; Sellers et al, 1986; Hicks et al, 1987; Dingman, 1994). The correction functions are:

$$g_R(\mathrm{PAR}) = \left(1 + \frac{b_{st}}{\mathrm{PAR}}\right)^{-1}, \tag{13}$$

$$g_\delta(\delta_q) = \begin{cases} 1 - 66.6\rho_a\delta_q & \text{for } \rho_a\delta_q \le 0.01152\ \mathrm{kg\,m^{-3}} \\ 0.233 & \text{for } \rho_a\delta_q > 0.01152\ \mathrm{kg\,m^{-3}} \end{cases}, \tag{14}$$

$$g_T(T_f) = \frac{T_f - T_{min}}{T_{opt} - T_{min}} \left\{ \frac{T_{max} - T_f}{T_{max} - T_{opt}} \right\}^{b_T}, \tag{15}$$

where b_{st} is a plant-specific constant (Table 1). The exponent b_T can be deduced from the derivation of $g_T(T_f)$ with respect to T_f and the optimum condition that $dg_T(T_f)/dT_f = 0$ and, hence, $T_f = T_{opt}$. One obtains

$$b_T = \frac{T_{max} - T_{opt}}{T_{opt} - T_{min}}. \tag{16}$$

The minimum and maximum temperatures marking the temperature range for which stomata should always be open are denoted by T_{min} and T_{max}, respectively, and T_{opt} is the temperature at which r_{st} reaches its minimum. Furthermore, the empirical relation (Dingman, 1994),

$$g_\eta(\Delta\eta) = \begin{cases} 1 - 0.00119\exp\left(81\sum_{j=1}^{k}\Delta z_j(\eta_{fc,j} - \eta_j)\right) & \text{for } \eta_j \le \eta_{fc,j} \\ 1 & \text{for } \eta_j > \eta_{fc,j} \end{cases} \tag{17}$$

accounts for the soil water deficit in the root zone. Here, Δz_j is thickness of the root containing soil layer j in meter, $\eta_{fc,j}$ is its field capacity, η_j is its actual volumetric water content, and k is the deepest layer where roots still exist (see also Sect. 2.3.1). Note that for $j = k$ only the fraction of the soil layer is considered that contains roots. For $\eta_{fc,j} < \eta_j$ water will percolate in macro-pores until field capacity is reached again.

The correction function for the concentration of CO_2 reads (e.g., Kramm, 1995)

$$g_{CO_2}(CO_2) = \begin{cases} 1, & \text{for } [CO_2] \le 100\,\mathrm{ppmv} \\ 1 - b_{c_1}, & \text{for } 100\,\mathrm{ppmv} < [CO_2] \le 1000\,\mathrm{ppmv} \\ b_{c_2}, & \text{for } [CO_2] > 1000\,\mathrm{ppmv} \end{cases}, \tag{18}$$

where b_{c_1} and b_{c_2} depend on the vegetation type. As suggested by Eq. (18), a long-term increase of the stomatal resistance may be a possible response of plants to an increase in the atmospheric CO_2 concentration (e.g., Dingman, 1994). A review on the impact of CO_2 on the stomatal resistance can be found, for instance, in Rosenberg et al (1989). Note that $[CO_2]$ is customarily presupposed or predicted in climate models. Since no measurements of $[CO_2]$ are available at Brandis, $g_{CO_2}(CO_2)$ is set equal to 1 for simplicity in this study.

2.1.2 Temperature and moisture at the surfaces of foliage and soil

The following coupled energy- and water-budget equations are used to calculate the values of temperature and moisture at the surfaces of foliage

and soil as required by Eqs. (1)–(4) (see Kramm, 1995; Kramm et al, 1996; Mölders, 1999),

$$F_1(\mathbf{S}) = R_{sf\downarrow} - R_{sf\uparrow} + R_{lf\downarrow} - R_{lf\uparrow} - R_{sg\downarrow} + R_{sg\uparrow} - R_{lg\downarrow} + R_{lg\uparrow} - H_f - L_v E_f = 0, \quad (19)$$

$$F_2(\mathbf{S}) = R_{sg\downarrow} - R_{sg\uparrow} + R_{lg\downarrow} - R_{lg\uparrow} - H_g - L_v E_g + G = 0, \quad (20)$$

$$F_3(\mathbf{S}) = I_g + W_{soil} - E_g = 0, \quad (21)$$

where $R_{sf\downarrow}$, $R_{sf\uparrow}$, $R_{lf\downarrow}$, $R_{lf\uparrow}$, $R_{sg\downarrow}$, $R_{sg\uparrow}$, $R_{lg\downarrow}$, and $R_{lg\uparrow}$ are the downward ($\downarrow$) and upward ($\uparrow$) directed fluxes of short-wave (index s) and long-wave (index l) radiation. Again the subscripts f and g represent the surfaces of foliage and soil. The global radiation, $R_{sf\downarrow}$, and the long-wave radiation of the atmosphere, $R_{lf\downarrow}$, can be delivered by simple parameterization schemes, sophisticated radiative transfer models or respective radiation sensors at the measuring site. The quantities $R_{lf\downarrow}$, $R_{sf\uparrow}$, $R_{lf\uparrow}$, $R_{sg\downarrow}$, $R_{sg\uparrow}$, $R_{lg\downarrow}$, and $R_{lg\uparrow}$ can be found in Deardorff (1978), Kramm (1995), and Mölders (1999). Furthermore, G and W_{soil} are the soil heat and water fluxes at the surface given by Kramm (1995), Kramm et al (1996), and Mölders (1999), and L_v is the latent heat of vaporization. Since HTSVS was developed within the framework of dry deposition studies (e.g., Kramm, 1995; Kramm et al, 1996) it included only a simple parameterization of infiltration, I_g. Therefore, for use of HTSVS in climate modeling, Mölders (1999) replaced this parameterization by an explicit formulation of the Green-and-Ampt-approach, in accord with Schmidt (1990). Furthermore, W_{soil} also contains the vertical transfer of water vapor across the soil layers. This soil water vapor flux is applied to estimate the bulk resistance of a certain soil layer against the transfer of trace gases, as required in studies on dry deposition and natural emission. Minor additions made to HTSVS are to accommodate (1) the effects of soil wetness on soil albedo, α_g, according to McCumber and Pielke (1981), and (2) that soil type may vary with depth. The set of the coupled nonlinear budget equations (19) to (21) is simultaneously solved by a Newton-Raphson iteration procedure of first-order (Kramm, 1995; Kramm et al, 1996; Mölders, 1999),

$$\mathbf{S}^{(n+1)} = \mathbf{S}^{(n)} - \mathrm{DF}(\mathbf{S}^{(n)})^{-1} \mathrm{F}(\mathbf{S}^{(n)}), \quad (22)$$

where $\mathbf{S} = \{T_f \;\; T_g \;\; \eta_g\}^T$ and $F(\mathbf{S}) = \{F_1(\mathbf{S}) \;\; F_2(\mathbf{S}) \;\; F_3(\mathbf{S})\}^T$. Here, DF($\mathbf{S}$) is the functional matrix, DF($\mathbf{S}$)$^{-1}$ is the corresponding inverse matrix, and T denotes the transpose. In contrast to Kramm (1995) and Kramm et al (1996), the elements of DF($\mathbf{S}$) are elementary derived (Mölders, 1999). The iteration procedure will stop if a sufficient accuracy of $|F_1(\mathbf{S}^{(k)})| < 0.1\,\mathrm{W\,m^{-2}}$, $|F_2(\mathbf{S}^{(k)})| < 0.1\,\mathrm{W\,m^{-2}}$, and $|F_3(\mathbf{S}^{(k)})| < 10^{-7}$ is achieved after the k-th iteration step. Usually, k amounts to five to six iteration steps. HTSVS is capable for calculating temperatures of the surfaces of foliage and soil that may differ from each other as really observed. Thus, the thermal stratification of the ASL can be predicted more accurately (for further details, see Mölders, 1999).

2.2 Snow-atmosphere interactions

Combining the Eqs. (3)–(5) and assuming $\sigma_f = 0$ provide the fluxes of sensible heat and water vapor over the snow,

$$H_s = -\frac{c_p \rho_a}{r_{mt,snow} + r_t}(\Theta_R - T_{snow,surf}), \quad (23)$$

$$E_s = -\frac{\rho_a}{r_{mt,snow} + r_t}(q_R - q_{snow,surf}), \quad (24)$$

where T_g, q_g, and $r_{mt,g}$ in Eqs. (3) and (4) have to be replaced by the quantities, $T_{snow,surf}$, $q_{snow,surf}$, and $r_{mt,snow}$ at the surface of the snow-pack, where $q_{snow,surf}$ is assumed to be at saturation with respect to ice.

Since in our study the stand-alone version of HTSVS will be driven by meteorological data, we use the snow water equivalent routinely recorded at Brandis. The snow depth, z_{snow}, is related to snow water equivalent by assuming a snow density of $100\,\mathrm{kg/m^3}$. A linear profile of snow temperature, T_{snow}, within the snow-pack is assumed. Thus, the heat flux into the snow-pack is given by

$$G_{snow} = -\lambda_{snow}\frac{T_{snow,surf} - T_g}{z_{snow}} - L_v \rho_w k_v \frac{(q_{snow,surf} - q_g)}{z_{snow}}. \quad (25)$$

Here, $\lambda_{snow} = 0.08\,\mathrm{W\,m^{-1}\,K^{-1}}$ is the thermal conductivity of snow (Oke, 1978), and k_v denotes the molecular diffusion coefficient of water vapor within air-filled pores of the snow-pack.

2.2.1 Temperature and moisture at the surfaces of snow and soil

The energy and water budgets of the snow-pack and the underlying soil read

$$F_1(\mathbf{S}) = R_{ss\downarrow} - R_{ss\uparrow} + R_{ls\downarrow} - R_{ls\uparrow} - H_s - L_sE_s + G_{snow} + P_H - R_{sg\downarrow} + R_{sg\uparrow} = 0, \quad (26)$$

$$F_2(\mathbf{S}) = R_{sg\downarrow} - R_{sg\uparrow} + G - G_{snow} = 0, \quad (27)$$

$$F_3(\mathbf{S}) = P + S - E_s - W_{soil} = 0, \quad (28)$$

where $S = \{ T_{snow,surf} \;\; T_g \;\; \eta_g \}^T$. Here, $R_{ss\downarrow}$, $R_{ls\downarrow}$, $R_{ss\uparrow}(=\alpha_{snow}\, R_{ss\downarrow})$, and $R_{ls\uparrow}$ are the downward and upward directed fluxes of short-wave and long-wave radiation comparable to $R_{sf\downarrow}$, $R_{lf\downarrow}$, $R_{sf\uparrow}$, and $R_{lf\uparrow}$. Furthermore,

$$R_{sg\downarrow} = R_{ss\downarrow} \exp(-k_{ext}\, z_{snow}), \quad (29)$$

and

$$R_{sg\uparrow} = \alpha_g R_{sg\downarrow} \quad (30)$$

are the downward and upward directed fluxes of short-wave radiation through the snow-pack to and from the ground, and k_{ext} ($=20\,m^{-1}$) is the extinction coefficient for snow. Moreover, P_H is the input of heat into the snow-pack by rain, S is the precipitation in solid phase, and L_s is the latent heat of sublimation. The temperature of rain is assumed to be equal to air temperature as commonly assumed in the cloud modules of climate models.

Snow albedo, α_{snow}, and emissivity, ε_{snow}, depend on snow age, t_{snow} in s, after the last snowfall event according to

$$\alpha_{snow} = \begin{cases} 0.35 + 0.18\exp\left(\frac{-t_{snow}}{114048}\right) \\ \quad + 0.31\exp\left(\frac{-t_{snow}}{954720}\right), & \text{for } T_R > T_0\,, \\ 0.61 + 0.23\exp\left(\frac{-t_{snow}}{469411}\right), & \text{for } T_R \le T_0 \end{cases} \quad (31)$$

$$\varepsilon_{snow} = \max(0.82, 0.99 - 9.8\cdot 10^{-7} t_{snow}). \quad (32)$$

Here, T_R is air temperature at z_R and $T_0 = 273.15\,K$ is the freezing point. These equations are derived from data cited by Dingman (1994). The set of the coupled nonlinear equations (26)–(28) is similarly solved like equation set (19)–(21).

2.3 The soil model

The treatment of the (vertical) heat- and water-transfer processes is based on the principles of the linear thermodynamics of irreversible processes (e.g., de Groot, 1951; Prigogine, 1961) including the Richards-equation (e.g., Philip and de Vries, 1957; Philip, 1957; de Vries, 1958; Kramm, 1995; Kramm et al, 1996; Mölders, 1999). Since the seasonally frozen soil affects the surface energy balance and the hydrologic response, a diagnostic approach to consider the effects of frozen soil was added to the diffusion equations for soil moisture and heat. The governing balance equations for heat and moisture including phase transition processes and water extraction by roots read

$$\frac{\partial \eta}{\partial t} = \frac{\partial}{\partial z}\left((D_{\eta,v} + D_{\eta,w})\frac{\partial \eta}{\partial z} + D_{T,v}\frac{\partial T_S}{\partial z} + K_w \right) - \frac{\chi}{\rho_w} - \frac{\rho_{ice}}{\rho_w}\frac{\partial \eta_{ice}}{\partial t}, \quad (33)$$

$$C\frac{\partial T_S}{\partial t} = \frac{\partial}{\partial z}\left((\lambda + L_v\rho_w D_{T,v})\frac{\partial T_S}{\partial z} + L_v\rho_w D_{\eta,v}\frac{\partial \eta}{\partial z} \right) + L_f\rho_{ice}\frac{\partial \eta_{ice}}{\partial t}, \quad (34)$$

where t is time, T_S is soil temperature in K, η is the soil volumetric water content, L_f is the latent heat of fusion, and $\chi = X/\Delta z$ is the water uptake by roots per soil volume, and $D_{\eta,v}$, $D_{\eta,w}$ as well as $D_{T,v}$ are the transfer coefficients with respect to water vapor, water, and heat according to de Vries (1958), Kramm (1995), Kramm et al (1996), and Mölders (1999). The volumetric heat capacity of moist soil,

$$C = (1-\eta_s)\rho_S c_S + \eta\rho_w c_w + \eta_{ice}\rho_{ice}c_{ice} + (\eta_s - \eta - \eta_{ice})\rho_a c_p, \quad (35)$$

depends on the porosity of the non-frozen soil, η_s, the density of dry soil, ρ_S, water, ρ_w, ice, ρ_{ice}, and air, the specific heat values of the dry soil material, c_S, water, c_w, and ice, c_{ice}, as well as the specific heat of air at constant pressure. For $T_S > T_0$ the heat conductivity, λ, is specified as a function of the water potential, Ψ (also

called matric potential, suction and tension head), by using McCumber and Pielke's (1981) empirical formula (see also Kramm, 1995; Kramm et al, 1996; Mölders, 1999). For $T_S \leq T_0$ a mass-weighted thermal conductivity depending on the amounts of liquid and solid volumetric water content present is calculated using the afore-mentioned thermal conductivity for the liquid and a value of 2.31 J/(msK) for the solid phase.

Obviously, the coupled equation set (33) and (34) generally includes cross-effects like the Ludwig-Soret effect (i.e., a temperature gradient contributes to the water flux and changes soil volumetric water content) and Dufour effect (i.e., a moisture gradient contributes to the heat flux and alters soil temperature). These equations are solved simultaneously by the Crank-Nicholson-scheme in conjunction with Gauß-Seidel-techniques. Before integrating, a logarithmic coordinate transformation is introduced into Eqs. (33) and (34) by $\xi = \beta \ln(z/z_D)$ to apply equal spacing and central differences for well appropriate finite difference solutions. Here, $z_D (= -8.25\,\mathrm{m}$ in our study) is the lower boundary, and β is a constant which is to be chosen for convenience.

2.3.1 Water extraction by roots

The water extraction by roots and the following transpiration act as a sink for soil water. This water uptake, $-X$, is described by Cowan's (1965) model further-developed by Federer (1979) and Martin (1990). Herein, the potential or maximum extraction of water from soil layer j by vegetation is given by (e.g., Federer, 1979; Martin, 1990),

$$X_j = \max\left(0, \sigma_f \rho_w \Delta z_j \frac{\Psi_j - \Psi_c - h}{r_r/L_j + \alpha_j/K_{wj}}\right), \qquad (36)$$

where Ψ_j is the water potential of soil layer j expressed by the empirical relation (e.g., Clapp and Hornberger, 1978),

$$\Psi = \Psi_s \left(\frac{\eta_s}{\eta}\right)^b = \Psi_s W^{-b}. \qquad (37)$$

Here, Ψ_s is the water potential at saturation, b is the pore-size distribution index (see Tab. 2), and $W = \eta/\eta_s$ is the relative volumetric water content. The quantities Ψ_c, h, and r_r are the water potential corresponding to the soil water potential at which the production of cytokinis by roots is sufficiently reduced to close stomata (Table 1), the height of canopy (see Fig. 1), and the internal vascular resistance per unit length of roots taken as $r_r = 5 \cdot 10^{12}\,\mathrm{s/m}$. Furthermore,

$$K_w = K_{ws} W^c, \qquad (38)$$

is the hydraulic conductivity of soil, K_{ws} is its value at saturation (Table 2), and $c = 2b + 3$ is the pore-disconnectedness index (e.g., Clapp and Hornberger, 1978; Dingman, 1994). Moreover, α_j is Cowan's (1965) root parameter that is determined in accord with Federer (1979), and Sellers et al (1986) by

$$\alpha_j = \frac{1}{8\pi L_j}\left(\delta_j - 3 - 2\frac{\ln \delta_j}{1 - \delta_j}\right). \qquad (39)$$

Here, δ_j is the volume of roots per unit volume of soil with respect to layer j. This quantity depends on the (oven-dry) fine root bio-mass, m_j, in layer j per unit area ($\mathrm{kg\,m^{-2}}$) and the average volumetric density of (oven-dry bio-mass of) roots, ρ_r (e.g., Martin, 1990),

$$\delta_j = \frac{m_j}{\rho_r \Delta z_j}, \quad \text{where } 0 < \delta_j < 1. \qquad (40)$$

Even though soil-physical and geologic characteristics, soil moisture, soil-temperature, aeration, competition or interaction with roots of other species, fertilizer, biologic and soil-chemical processes affect the distribution of roots, roots are assumed to be uniformly spaced within a soil layer in accord with other authors (e.g., Gardner, 1960; Cowan, 1965; Federer, 1979; Martin, 1990). The rooting density (i.e., the length of roots per unit volume of soil in $\mathrm{m/m^3}$) in the layer j is given by (e.g., Federer, 1979; Martin, 1990)

$$L_j = \frac{\delta_j}{\pi R_{r,j}^2}, \qquad (41)$$

where $R_{r,j}$ is the mean root radius (Table 1).

In contrast to Federer's (1979) and Martin's (1990) root parameterization, the vertical distribution of roots in the upper layers of soil differs from that in the layers below (Fig. 2). Two cases can be distinguished. First, the fine root bio-mass

Table 2. Soil profile characteristics as used in our study. Here, K_{ws}, η_s, b, Ψ_s, and $c_S\rho_S$ are the saturated hydraulic conductivity, porosity (saturated volumetric water content), pore-size distribution index, saturation potential, and dry volumetric heat capacity of the soil material. Values are deduced from the pf-curve, from grain size, grain-size and pf-curve, and under consideration of grain-size, pf-curve and skeletton of the soil, respectively. See text for further explanation

Soil layer	K_{ws}	η_S	b	Ψ_s	$c_S\rho_S$
m	10^{-4} m/s	m^3/m^3	-.-	m	10^5 Jm^{-3} K^{-1}
0.000–0.025	1.800	0.400 (0.360, 0.360, 0.400)	2.84 (2.41, 2.6, 3.82)	− 2.09 (− 2.21, − 2.12, − 0.62)	9.34336
0.025–0.052	1.800	0.400 (0.360, 0.360, 0.400)	2.84 (2.41, 2.6, 3.82)	− 2.09 (− 2.21, − 2.12, − 0.62)	9.34336
0.052–0.107	1.800	0.400 (0.360, 0.360, 0.400)	2.84 (2.41, 2.6, 3.82)	− 2.09 (− 2.21, − 2.12, − 0.62)	9.34336
0.107–0.220	1.800	0.400 (0.360, 0.360, 0.400)	2.84 (2.41, 2.6, 3.82)	− 2.09 (− 2.21, − 2.12, − 0.62)	9.34336
0.220–0.454	1.978	0.382 (0.360, 0.360, 0.382)	3.00 (2.47, 2.65, 3.51)	− 1.22 (− 2.00, − 1.94, − 0.36)	8.79037
0.454–0.938	2.200	0.360 (0.360, 0.360, 0.360)	3.21 (3.33, 3.33, 3.13)	− 0.13 (− 0.39, − 0.40, − 0.03)	8.10000
0.938–1.936	1.995	0.367 (0.371, 0.371, 0.367)	3.11 (3.41, 3.41, 3.06)	− 0.19 (− 0.26, − 0.26, − 0.09)	8.16064
1.936–3.996	1.127	0.400 (0.430, 0.430, 0.400)	2.77 (2.93, 2.93, 2.81)	− 0.48 (− 0.28, − 0.18, − 0.34)	8.63047
3.996–8.250	1.100	0.400 (0.420, 0.420, 0.400)	2.71 (2.87, 2.87, 2.75)	− 0.47 (− 0.27, − 0.18, − 0.34)	8.42600

of layer j depends on the total fine root bio-mass, m, according to

$$m_j = m \begin{cases} a & z_j \geq z_d \\ \frac{a(|z_d|-|z_j|+\Delta z_j)+(2-a)(|z_j|-|z_d|)}{\Delta z_j} & z_{j-1} > z_d \geq z_j \\ 2-a & z_{j-1} > z_j \geq z_{root}, \\ \frac{(2-a)(|z_{root}|-|z_j|+\Delta z_j)}{\Delta z_j} & z_{j-1} > z_{root} \geq z_j \\ 0 & z_{root} > z_{j-1} \end{cases} \quad (42)$$

where a is the fraction of roots in the upper part of soil (Table 1). In this study, the upper part extends to a depth, z_d, which is taken to be at -0.1 m. The maximum root depth, z_{root}, is assumed to be always below this layer, i.e. minimum root depth is equal to 0.11 m.

In the second case, maximum root depth falls into the layer where z_d is located. Then, the fine root bio-mass of layer j reads

$$m_j = m \begin{cases} a & z_j \geq z_d \\ \frac{a(|z_d|-|z_j|+\Delta z_j)+(2-a)(|z_j|-|z_d|)}{\Delta z_j} & z_{j-1} > z_d \\ & > z_{root} \geq z_j \\ 0 & z_{root} > z_{j-1} \end{cases}. \quad (43)$$

Equations (42) and (43) realize that the root distribution in the upper root space differs from that in the lower one. In the soil layer, which includes the boundary between the upper and lower root space, the root biomass is weighted accordingly. If the roots end in a layer, the root mass will be accounted in accord with the root length. In doing so, the vertical root profile can be specified by up to four different values. Most LSMs assume an equal distribution of roots in the root zone or only distinguish between the upper and lower root space under the assumptions that the boundary between the two root spaces as well as the maximum root length fall together with a soil layer boundary (e.g., Wilson et al, 1986; Martin, 1990).

When the wilting point, $\eta_{pwp} = \eta_s(\Psi_s/\Psi_{pwp})^{1/b}$, which is deduced from Eq. (37) by assuming a water potential of $\Psi_{pwp} = -150$ m (Dingman, 1994; Marshall et al, 1996), water extraction continues at a reduced rate until the water potential goes down to $\Psi_{inf} = -500$ m (Gardner and Ehlig, 1963). This phenomenon is attributed by

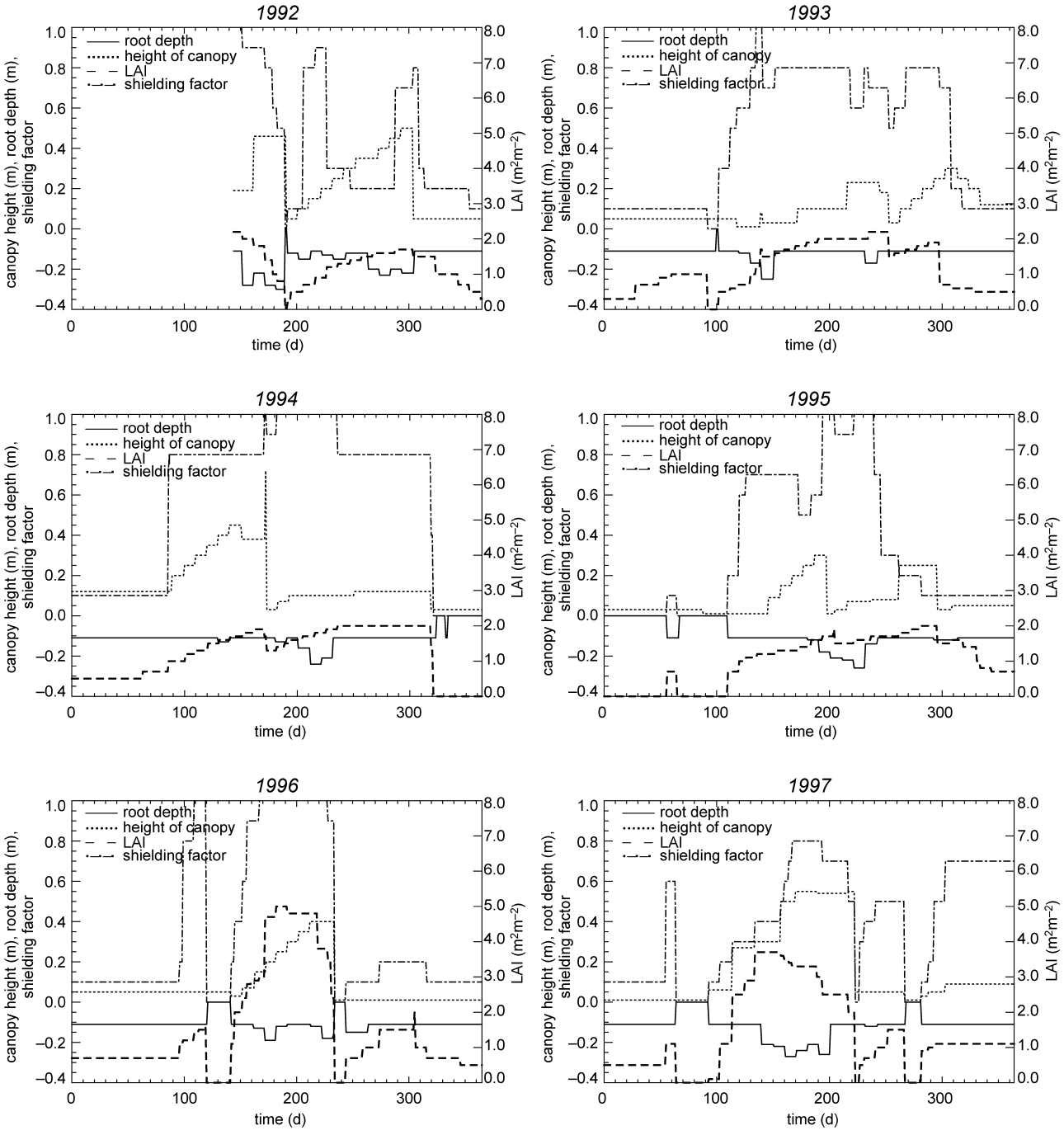

Fig. 1. Temporal development of maximum root depth (solid lines), LAI (dashed lines), shielding factor, (dashed dotted lines), and canopy height (dotted lines) for six consecutive years. The vegetation types are winter barley (1992), green fallow (1993; 1994), red clover (1995), potatoes (1996), and summer wheat (1997) with green fallow growing after the harvest of barley, potatoes, and summer wheat. Note that canopy height only slightly differs over the field. For the vegetation parameters see Table 1

an empirical approach based on Gardner and Ehlig's (1963) data (Martin, 1990),

$$X_j = \max(0, X_{pwp,j}(\eta_j - \eta_{pwp,j})/(\eta_{inf} - \eta_{pwp,j})), \quad (44)$$

where $X_{pwp,j}$ is the water extraction in layer j at wilting point, and $\eta_{inf} = \eta_s(\Psi_s/\Psi_{inf})^{1/b}$ is the lowest volumetric water content for which extraction occurs also deduced from Eq. (37).

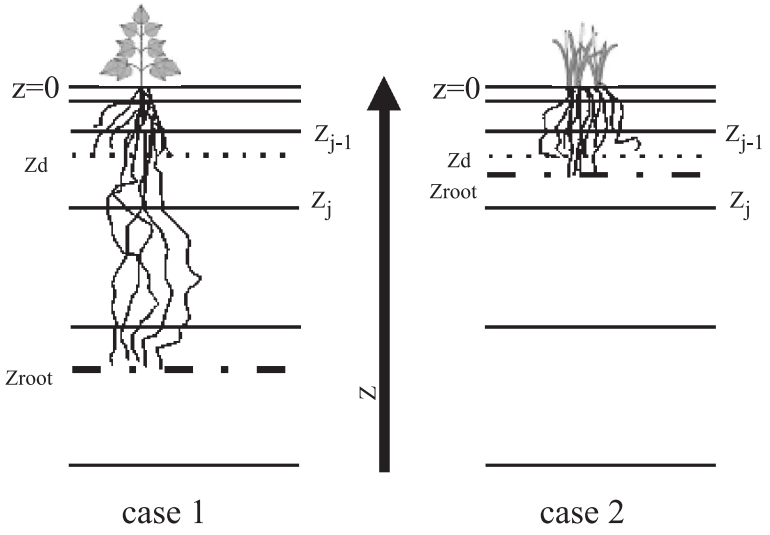

Fig. 2. Schematic view of the root system as realized in HTSVS. In case 1, the roots extend into deeper layers than the layer of the boundary, z_d, between the upper and lower root zone. In case 2, maximal root depth falls into the layer where z_d is located. See text for further explanation

Equation (36) determines the maximum potential extraction of water that can be taken from layer j by roots. The amount of water, w, that can really be taken up per unit area of one square meter from layer j depends on the volumetric water content of that layer (e.g., Martin, 1990),

$$w_j = \rho_w \Delta z_j (\eta_j - \eta_{inf}). \tag{45}$$

Thus, $X_{max,j} = w_j/\Delta t$ is the actual amount of water that can be extracted per time step per unit area from layer j, i.e., it corresponds to a water flux density. Consequently, the actual water flux from layer j is given by (e.g., Martin, 1990)

$$X_{min,j} = \min(X_j, X_{max,j}). \tag{46}$$

The share of potential supply of available water from layer j with respect to the total potential water supply across all layers, $j = 1, \ldots, k$, is determined by (e.g., Martin, 1990)

$$\nu_j = \frac{X_j}{\sum_{j=1}^{k} X_j}. \tag{47}$$

The effective evaporative flux due to transpiration per unit area from layer j may, therefore, be calculated by (e.g., Martin, 1990)

$$e_j = \min(\nu_j \sigma_f E_f, X_j). \tag{48}$$

The sum of the effective evaporative fluxes due to vegetation must equal the transpiration,

$$\sum_{j=1}^{k} e_j = E_f, \tag{49}$$

given by Eq. (2).

2.3.2 Frozen soil

When ice is present, the soil water potential, Ψ, remains in equilibrium with the vapor pressure over pure ice. It can be expressed by (Fuchs et al, 1978)

$$\Psi = \pi + \frac{L_f(T_S - 273.15)}{gT_S}, \tag{50}$$

where π is the osmotic potential, and g is the acceleration of gravity. Osmotic effects due to solutes are omitted from the original equation because HTSVS does not deal with solute chemistry at present. The volumetric ice content, η_{ice}, is defined by the difference of the total water within the soil layer, $\eta_{total} = \eta_{max} + \frac{\rho_{ice}}{\rho_w}\eta_{ice}$, minus the maximum liquid water content for temperatures below freezing point,

$$\eta_{max} = \eta_s \left\{ \frac{L_f(T_S - 273.15)}{g\Psi_s T_S} \right\}^{-1/b}. \tag{51}$$

Since the phase transition alters the soil temperature by release or consumption of heat, Eq. (51) has to be solved iteratively by a first-order Newton-Ralphson-technique. Figure 3 exemplary illustrates the dependence of maximum liquid water content on soil temperature for some of the soil types used in our study (Table 2). Ice changes the dynamics of soil thermal fluxes through the dependence of soil thermal conductivity and volumetric heat capacity on volumetric water and ice content of the soil.

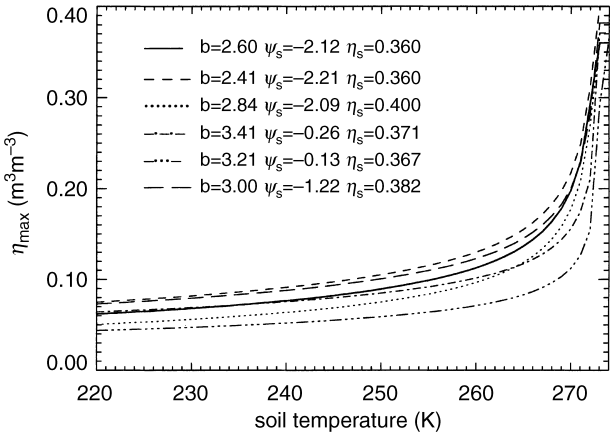

Fig. 3. Dependence of maximum liquid water content on soil temperature for some of the soil types listed in Table 2

3. Design of the study

Besides the specification of parameters that characterize the land surface and soil types the stand-alone version of HTSVS requires the input of atmospheric forcing data to perform off-line simulations. These data are described in sections 3.1 to 3.4. Since the aim of our study is to evaluate the impact of root water uptake, snow, and soil frost on the long-term water budget quantities and soil temperature, results from simulations with and without parameterizations of these processes are compared and analyzed. The impact of the root parameterization is examined in more detail by alternatively considering (1) the land-use grown on the lysimeters and (2) grass because water uptake by roots varies with vegetation type. Since the soil temperatures were measured at the climate station covered by grass, results of simulations assuming grassland are used in evaluating predicted soil temperatures. To evaluate the accuracy and sensitivity of the frost parameterization, simulations are performed using different parameterizations of downward directed long-wave radiation and the various sets of values determined for the soil physical parameters (Tables 2 and 3).

3.1 Meteorological forcing

At Brandis, routine data of hourly mean values of wind, relative humidity, temperature, global radiation, and precipitation are continuously available from May 23, 1992 to December 31, 1997 that amounts to 2050 days. Soil temperatures are monitored at 0.05 m, 0.1 m, 0.2 m, 0.5 m depth and since May 10, 1996 also at 1 m, and 2.5 m depth. As the original data set at the climate station does not include downward long-wave radiation, $R_{lf\downarrow}$ or $R_{ls\downarrow}$, this quantity is

Table 3. 2050-days-accumulated sums of water supply to the atmosphere and recharge as obtained from the various simulations. See text for description of simulations

Simulation	Water supply to the atmosphere mm	Recharge mm
Observation	2966.4	941.0
Reference simulation	3177.5	1006.6
Without roots	3200.1	1340.7
$z_d = 0.3$ m	3198.0	955.3
Without snow effects	3212.4	883.6
$\rho_{snow} = 400\,kg/m^3$	3259.5	1008.6
Without soil frost	2906.9	928.7
Granulation	3009.4	826.2
Without soil frost, granulation	2865.9	891.8
pf-curve and granulation	3111.9	916.4
Without soil frost, granulation, pf-curve	2943.8	912.3
pf-curve, granulation, skeleton	2255.0	1078.3
Without soil frost, pf-curve, granulation, skeleton	2906.9	928.7
$R_l\downarrow$ Idso and Jackson (1969)	3710.5	682.7
$R_l\downarrow$ Croley (1989)	4040.6	690.9
$R_l\downarrow$ Eppel et al (1995)	3431.7	854.9
Grass all the time	2304.2	1083.1
Without new parameterizations	2759.3	959.4

alternatively parameterized in accord with: (a) Bolz and Falkenberg (1949, denoted as B&F-scheme) by

$$R_{lf\downarrow} = R_{ls\downarrow} = \sigma T_a^4 (0.52 + 0.065 e_a^{0.5})(1 + 0.22 c^2), \quad (52)$$

(b) Idso and Jackson (1969, denoted as I&J-scheme) by

$$R_{ls\downarrow} = \frac{\sigma}{\varepsilon_s}\{(\varepsilon_s - 1)T_s^4 + (\varepsilon_a(1-c)+c)T_a^4\}, \quad (53)$$

$$R_{lf\downarrow} = \frac{\sigma}{\sigma_f \varepsilon_f + (1-\sigma_f)\varepsilon_g}\{\sigma_f(\varepsilon_f - 1)T_f^4 + (1-\sigma_f)(\varepsilon_g - 1)T_g^4 + (\varepsilon_a(1-c)+c)T_a^4\}, \quad (54)$$

with

$$\varepsilon_a = 1 - 0.261 \exp(-7.77 \cdot 10^{-4}(273 - T_a)^2), \quad (55)$$

(c) Eppel et al (1995, denoted as EEA-scheme) by

$$R_{ls\downarrow} = \left\{(1-c)\varepsilon_a + c\left(\varepsilon_a + (1-\varepsilon_a)\left(1 - \frac{53.6}{T_S}\right)\right)\right\}\sigma T_a^4, \quad (56)$$

$$R_{lf\downarrow} = \left\{(1-c)\varepsilon_a + c\left(\varepsilon_a + (1-\varepsilon_a)\left(1 - \frac{53.6}{\sigma_f T_f + (1-\sigma_f)T_g}\right)\right)\right\}\sigma T_a^4 \quad (57)$$

with

$$\varepsilon_a = 0.65 + 5.95 \cdot 10^{-7} \frac{q_v p}{0.623} \exp\left(\frac{1500}{T_a}\right), \quad (58)$$

and (d) Croley (1989, denoted as C-scheme) by

$$R_{ls\downarrow} = \sigma\{(1-\varepsilon_s)\varepsilon_a T_a^4 + \varepsilon_s T_s^4\}, \quad (59)$$

$$R_{lf\downarrow} = \sigma\{(\sigma_f \varepsilon_f + (1-\sigma_f)\varepsilon_g)(1-\varepsilon_a)T_a^4 + \sigma_f T_f^4 + (1-\sigma_f)T_g^4\} \quad (60)$$

with

$$\varepsilon_a = (0.53 + 0.065 e_a^{0.5})(1 + 0.4c). \quad (61)$$

The latter three approaches are presented in their forms adapted for HTSVS. Here, T_a and e_a are the observed air temperature, and water vapor pressure, respectively. Data of cloud cover, c, are taken from a nearby station. Emissivity of soil is assumed to be equal to 0.95 (see Oke, 1978; Pielke, 1984). Note that the B&F-scheme is favored in our study because it only bases on observed quantities, i.e., it is independent of simulated values (e.g., surface temperature) and presupposed usually not observed parameters (e.g., emissivity) as do the other three parameterizations.

3.2 Soil physical data, initial soil temperature and volumetric water content

Porosity, field capacity, and permanent wilting point were determined by four different methods, namely the granulation-method, pf-curve-method, a combined granulation-pf-curve-method, and a combined granulation-pf-curve-method under consideration of the soil skeleton (e.g., Keese et al, 1997; Haferkorn, 2001; Table 2). Specific heat capacity of soil material is deduced from the weighted average of the fraction of particle size and humus (Table 2).

In our study, the moisture and temperature, the water extract by roots as well as the transfer of water and heat are predicted on nine logarithmically spaced layers (see Table 2). Soil temperatures in 0.05 m, 0.1 m, 0.2 m, and 0.5 m depth and meteorological data of May 23, 1992 serve as initial conditions. Lysimeter data also available at Brandis serve to initialize soil volumetric water content. Note that the soil at the climate station is of similar properties as that in the lysimeter. At $z_D(= -8.25\,\text{m})$, a mean annual course of soil temperature is prescribed and the volumetric water content is held constant at field capacity.

3.3 Plant physiological data

In the adjacent field, lysimeters were run for which routine data of maximum root length, canopy height, and plant phenology is available about every ten days (Haferkorn, 2001). In the

period covered by our study, winter barley (1992), green fallow (1993; 1994), red clover (1995), potatoes (1996), and summer wheat (1997) were grown. Green fallow grew on the lysimeters after the harvest of barley, potatoes, and summer wheat. Shielding factor and LAI (Fig. 1) are deduced from the reported phenologic characteristics using an empirical relationship between phenologic description and LAI. These data are used in the reference simulation.

Except for the simulations assuming grass only, the vegetation-type changes according to the field management (Fig. 1). Maximum root depth, LAI, and canopy height, h, which is used, for instance, to determine roughness length z_0 ($=0.1\,h$) and zero plane displacement d_0 ($=0.7\,h$) in accord with Oke (1978) and Kramm (1989; 1995), are updated whenever new routine data are available (Note that z_0 and d_0 are required in the calculation of the stability functions.). The simulations performed with these land-use types serve to examine the impact of roots. In the simulations assuming grass only, the parameters given in Table 1 are applied throughout the entire integration except for snow events.

3.4 Snow depth data

Data of daily snow water equivalent are available for the 76 reported snow days. Snow depth is related to the snow water equivalent assuming a snow density of $100\,kg/m^3$ as customarily used in hydrometeorology (e.g., Dingman, 1994).

4. Results and discussion

The reference simulation (Table 3) is carried out with HTSVS including the parameterizations for water uptake by roots, snow and soil frost effects. Since data from combined methods are seldom available for large-scale areas as typical in climate models, the soil data derived from pf-curve are applied. The B&F-scheme and the land-use types as shown in Fig. 1 are used in the reference.

4.1 Downward directed long-wave radiation

The downward directed long-wave radiation predicted by the various schemes absolutely differs up to $143.2\,Wm^{-2}$ (Fig. 4; Table 4). Differences vary during the annual cycle. In winter, the downward directed long-wave radiation, $R_{lf\downarrow}$ (or $R_{ls\downarrow}$), provided by the B&F-scheme is, on average, about $50\,Wm^{-2}$ lower than those determined with the parameterizations which include surface properties (cf. Fig. 4). Compared to these parameterizations, the lower values of $R_{lf\downarrow}$ (or $R_{ls\downarrow}$) of the B&F-scheme are responsible for the higher frequency of days predicted with soil temperatures below freezing point (Table 5).

In comparing of simulated and observed soil temperatures only results from simulations performed for grass are applied because grass is the land-use type at the climate station. Soil temperatures below freezing point were observed on 66, 47 and 8 days in 0.05 m, 0.1 m and 0.2 m depth, respectively (Table 5). Obviously, the frequency of days with $T_0 < T_S$ predicted with the B&F-scheme is too high as compared to the observations. The opposite is true for the other schemes. Predicted and observed frequencies of such days agree the best for the C-scheme. Using only the observed air temperature (B&F-scheme) to calculate $R_{lf\downarrow}$ (or $R_{ls\downarrow}$) leads to an underestimation of surface and soil temperatures and an overestimation of frost depth.

Some of the discrepancies in that frequency may also result from the fact that the meteorological quantities like wind speed, air temperature, and humidity observed at the climate station are affected by the properties of its weather-side region; whereas global radiation, precipitation, and soil properties are representative only for the close vicinity of the climate station that generally provides routine data. Discrepancies may also stem from the disturbed soil texture, which results from digging the temperature-sensors in. The lack of long-wave radiation measurements and the facts discussed before may be responsible for the offset of 2 K between the predicted and measured soil temperatures found in our study (e.g., Fig. 5). Under such circumstances an offset of 2 K or so may be classified as a ''procedural error'' that has to be expected in long-term studies, even if sophisticated LSMs are applied (e.g., Flerchinger and Hanson, 1989; Cherkauer and Lettenmaier, 1999; Boone et al, 2000).

The predicted water budget quantities show a considerable sensitivity to the parameterization of

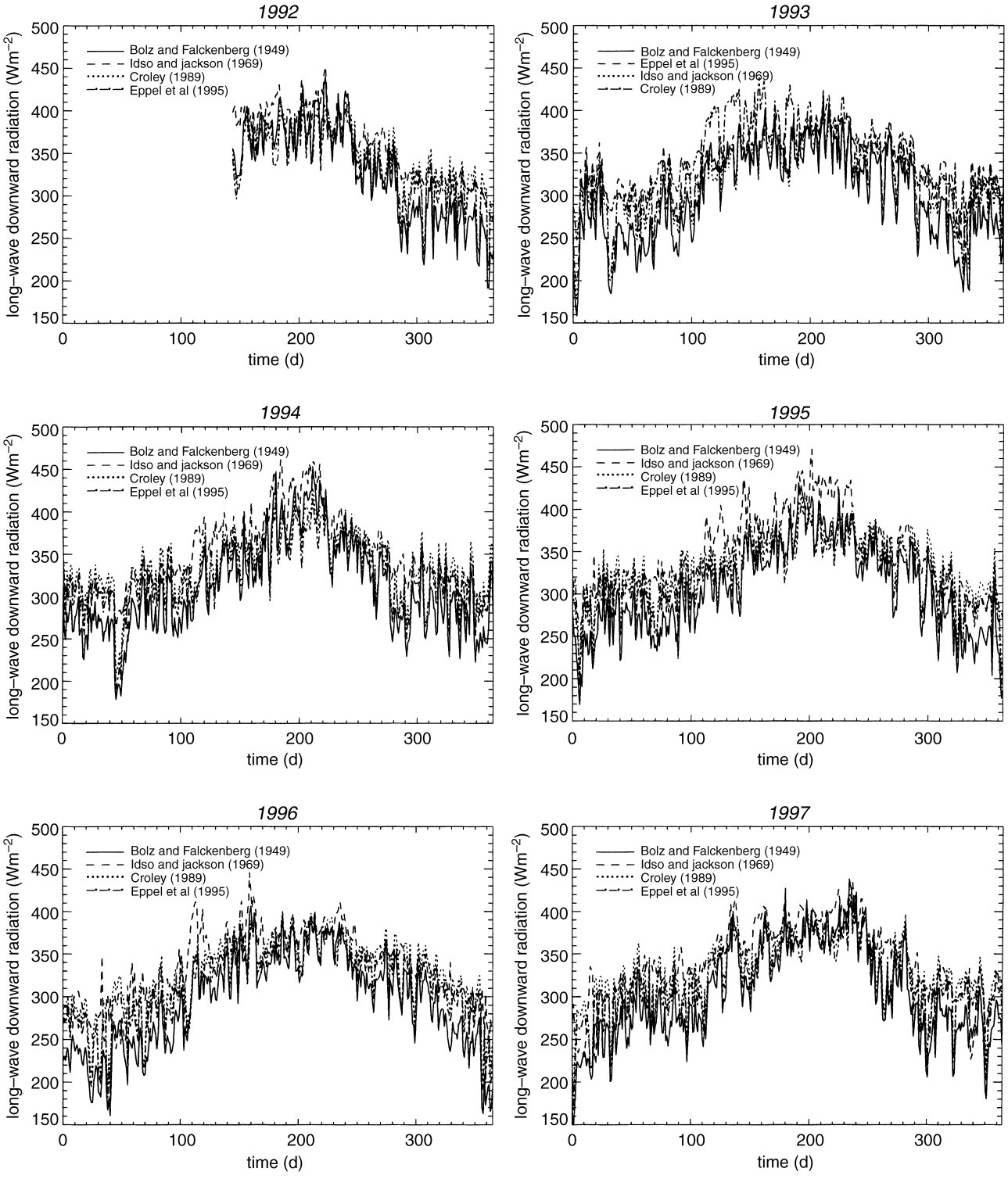

Fig. 4. Comparison of long-wave downward radiation as obtained by the various semi-empirical approaches discussed in the text. Note that Bolz and Falckenberg's approach (1949) is used in the reference simulation

downward directed long-wave radiation (Table 3). The impact is similar to that found for various LSMs by Schlosser et al (2000). Consequently, measurements of downward and upward long-wave radiation are indispensable for evaluating LSMs.

Table 4. Maximum and minimum differences in downward directed long-wave radiation in Wm^{-2}

Parameterization	Bolz and Falckenberg (1949)	Idso and Jackson (1969)	Croley (1989)	Eppel et al (1995)
Bolz and Falckenberg (1949)	0	− 63.6	− 143.2	− 58.9
Idso and Jackson (1969)	36.2	0	− 101.3	− 28.1
Croley (1989)	48.2	114.4	0	− 126.4
Eppel et al (1995)	46.8	9.9	83.8	0

Table 5. Frequency of days with soil temperatures below freezing point predicted with the various schemes to calculate $R_{lf\downarrow}$ (or $R_{ls\downarrow}$) versus observations performed at three different depths

Depth	Schemes				Observation
(m)	B&F	1&J	EEA	C	
	(days with soil temperatures below freezing point)				
0.05	118	28	28	48	66
0.10	108	16	18	34	47
0.20	75	6	5	11	8

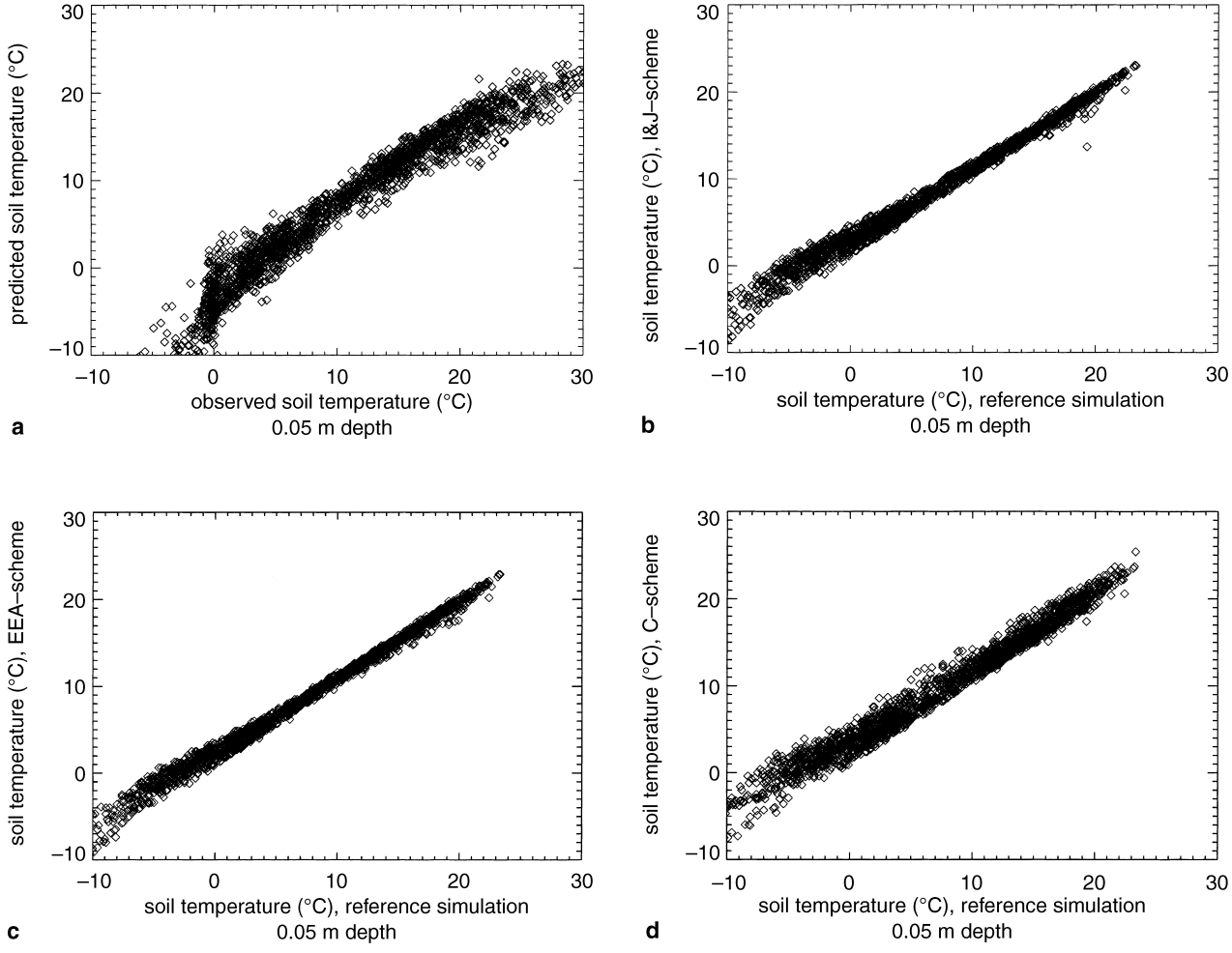

Fig. 5. Comparison of daily averaged predicted and observed soil temperatures as obtained with (**a**) the B&F-scheme, and comparison of soil temperatures predicted by the B&F-scheme (reference simulation) with results from simulations with (**b**) the I&J-scheme, (**c**) the EEA-scheme, and (**d**) the C-scheme all at a depth of 0.05 m

4.2 Effects of roots, Ludwig-Soret and Dufour effects

Except for the uppermost soil layer, taking root water uptake into account leads to, on average, slightly drier soils in the entire root space as compared with the simulation with no root effects (e.g., Fig. 6). Even though the daily differences in soil moisture and water fluxes are small, inclusion of roots notably affects the predicted accumulated sums of the water supply to the atmosphere, and recharge (Table 3). The reason for the relatively small effects on the short-time scale (several days) is that here only low vegetation is considered. Obviously, differences of the previous year propagate (e.g., Fig. 6).

On average, the water uptake by roots reduces the downward directed soil moisture flux. Since roots act as a sink of soil water in the root zone (e.g., Fig. 6), there is a gradient in volumetric water content in the immediate vicinity of the lower boundary of the root zone as compared to the case without root effects. To compensate this gradient the upward/downward moisture fluxes are enhanced/diminished in comparison to the no-root-effect simulations. These altered soil moisture fluxes are responsible for the over-proportional reduction in recharge as compared to the increase in evapotranspiration or to the recharge obtained in the simulations without root parameterization (Table 3).

In nature, root distribution, among other things, depends on depth, vertical distribution of soil water deficit, soil density, fertilizer, soil and vegetation (see also Fig. 1). The parameterization of root distribution allows either more roots in the upper or lower root zone where the boundary between the root zones is arbitrarily chosen to be in 0.1 m (cf. Fig. 2). A shift of this depth means another weighting from where the soil water is taken up (cf. Eqs. (42) and (43)). The resulting distribution of η leads to altered gradients of that quantity and, hence, altered soil moisture and heat fluxes as well as soil temperatures (e.g., Fig. 7). Similar differences in soil temperature are also found for the simulations with and without root effects. Results from simulations with and without consideration of the

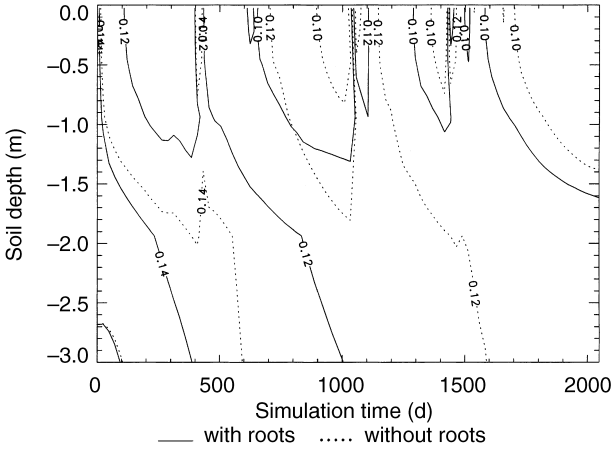

Fig. 6. Comparison of daily averaged volumetric soil water content as obtained by the simulations with and without consideration of root effects for the entire simulation time

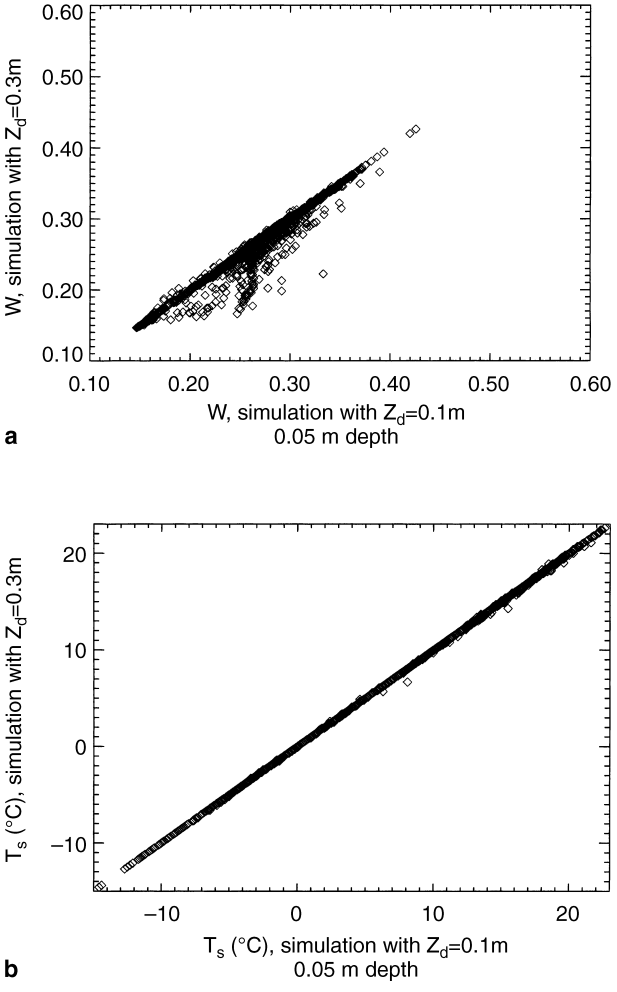

Fig. 7. Comparison of daily averaged (**a**) soil volumetric water content, and (**b**) soil temperature as obtained from the simulations assuming 0.1 m and 0.3 m as the depths for the partitioning between the upper and lower root zone. The scatter in soil temperatures provides a hint for how the Dufour- and Ludwig-Soret effects work on the long-term. See text for further discussion

Ludwig-Soret and/or Dufour-effect show similar differences in soil moisture and soil temperature. Thus, the effect of the boundary between the upper and lower root space is shown here exemplary to demonstrate the Dufour-effect. It is noteworthy that the choice of the boundary affects the 2050-day-sums of recharge and water supply to the atmosphere by about 5% each (cf. Table 3).

Based on these results, we conclude that (1) the Dufour- and Ludwig-Soret effects play a notable role on the long-term water budgets of soil and energy budgets, and (2) the vertical distribution of roots also affects both budgets. Thus, climate modeling requires global data sets on the annual course of root distribution for the various vegetation types.

4.3 The effects of snow

Figure 8 exemplary shows soil temperatures predicted with and without consideration of snow effects for the first two snow episodes of our data set. The snow water equivalents amount to 15.2 mm and 4.6 mm, respectively. This comparison elucidates that the insulating effect of snow reduces soil cooling down to a depth of about 1 m, i.e. soil frost occurs quite more often when snow insulating effects are ignored. At that depth, soil temperatures still differ long after the snow event (Fig. 8).

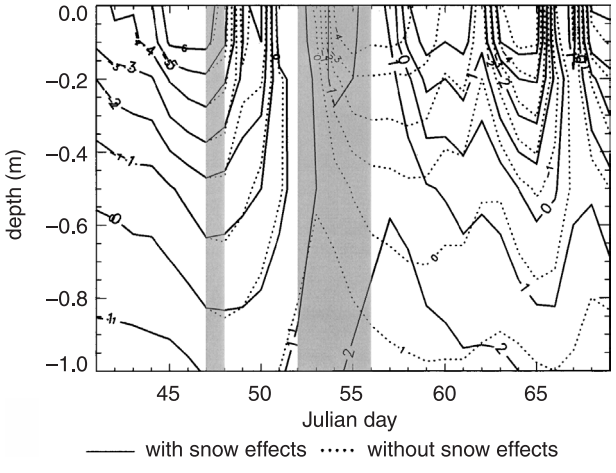

Fig. 8. Comparison of daily averaged soil temperatures as obtained from the simulations with and without consideration of snow effects from 10 February (41 Julian day) to 10 March 1993 (69 Julian day). Days with observed snow coverage are shaded in gray. Note that this time frame covers the first two snow episodes of our data set

The snow effects slightly delay recharge and increase accumulated recharge by about 12% (see also Table 3). Predicted accumulated water supply to the atmosphere is slightly reduced (about 1%) by consideration of snow effects (Table 3). This reduction may be explained by the greater amount of energy required for sublimation of snow than for evapotranspiration of water.

Wind blowing effects and snow metamorphism (wind break, water vapor diffusion from convex to concave surfaces and from warm to cold layers, gravity, percolation and re-freezing of melt-water) increase snow density (e.g., Dingman, 1994). Thus, the snow depth calculated from the measured snow water equivalent by assuming a snow density of $100\,kg/m^3$ may differ from the real snow depth. For a given snow water equivalent the snow depth decreases when the snow density increases. The results from simulations with a snow density of $400\,kg/m^3$ indicate, therefore, that the frequency of soil temperatures below freezing point increases as snow density grows. Snow density, of course, hardly (less than 3 mm in 2050 d) affects recharge (Table 3). Compared to this change in recharge the greater impact of snow on the water supply to the atmosphere is due to the modified snow temperature that results in response to the thinner snow layer. It has to be expected that under the consideration of snow metamorphism processes (e.g., Fröhlich and Mölders, 2002) a time varying snow density and, hence, retention of melt-water in the snow-pack may strongly influence recharge.

4.4 Soil frost

Since at the climate station the vegetation is grass, soil temperatures predicted by simulations assuming grassland for the entire time are compared to those observed. HTSVS well reproduces the propagation of soil cooling. While the overall prediction is satisfactory (e.g., Fig. 9), there are some weaknesses. As compared to the soil temperatures observed, HTSVS sometimes freezes the soil too early and too long, but the severity of this error depends on the semi-empirical approach applied for downward long-wave

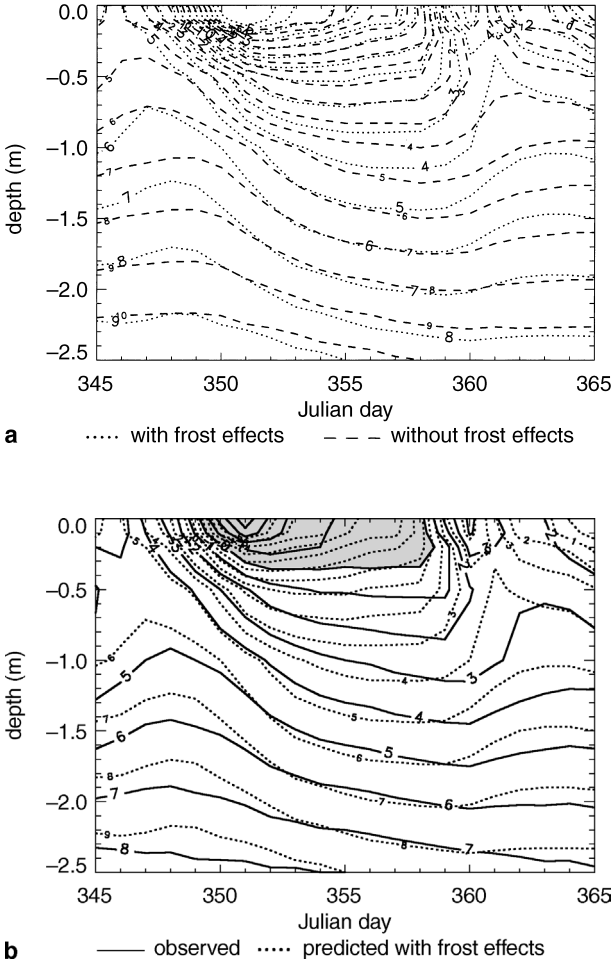

Fig. 9. Comparison of daily averaged soil temperatures as (**a**) obtained from the simulations with and without parameterization of soil frost effects, and (**b**) observed at the Brandis climate station from 11 to 31 December 1997. The gray shaded area denotes to observed soil frost. Note that prior soil frost events cause the differences between the simulations with and without soil frost seen on Julian day 345

radiation (see also Sect. 4.1 and Table 4). Slater et al (1998) found similar results for the LSM BASE (Best approximation of surface exchange). Figure 9 exemplary illustrates that previous frost events still affect deep soil temperatures long after they occurred. Ignoring soil frost yields an overestimation of about 1 K even at 2.5 m depth (Fig. 9). Compared to observations inclusion of soil frost improves the prediction, but there is still an overestimation of about 0.5 K at this depth. The simulations with and without frost parameterization performed with the other schemes for long-wave downward radiation also lead to a difference of about 1 K in soil temperature at 2.5 m except for the I&J-scheme where the frost effects are much smaller. When using the I&J-scheme, C-, or EEA-scheme the 2.5 m-soil temperature is overestimated up to 2.5 K, 2 K, and 2.5 K compared to the observations.

The simulations with surface temperature dependent parameterizations of long-wave downward radiation (I&J-, C-, EEA-scheme), which better predict the soil frost frequency, yield to a worse prediction of recharge and water supply to the atmosphere than that with the B&F-scheme (e.g., Table 3).

Figure 10 exemplary elucidates the effects of soil freezing on η. Freezing holds the water in the soil, and at the same time, reduces the water supply to the atmosphere. These results well agree with those reported by Cherkauer and Lettenmaier (1999).

Since the maximum liquid water that can be present at temperatures below freezing point depends on the soil parameters, soil ice prediction is highly sensitive to the determination of the soil parameters (cf. Fig. 3). Thus, depending on the determination of soil parameters the same soil frost parameterization leads to a slightly different frequency of soil frost events.

Using the parameters derived by the combined pf-curve and granulation method (Table 2) leads to a higher frequency of soil temperatures below freezing point except for 1 m depth than for applying the parameters determined otherwise. The way of determining the soil parameters slightly affects accumulated recharge and water

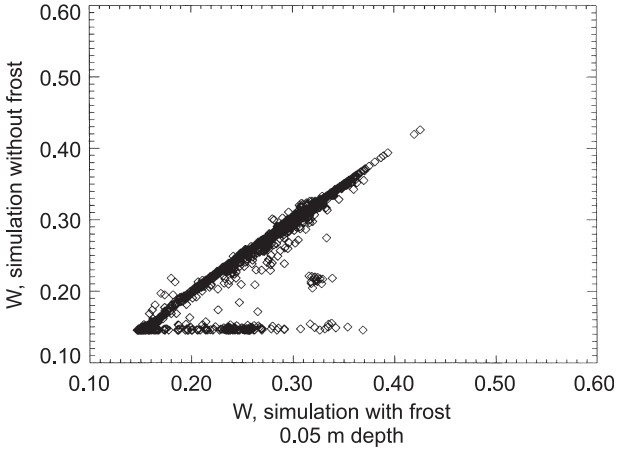

Fig. 10. Comparison of relative soil volumetric water content as predicted by the simulations with and without soil frost parameterization for the first soil frost episode of our study

supply to the atmosphere (Table 3). Applying the parameters gained by the granulation method also increases soil temperatures below T_0 except at 1 m depth.

5. Conclusion

The hydro-thermodynamic soil-vegetation-atmosphere transfer scheme HTSVS, which is a process model based on the principles of the linear thermodynamics of irreversible processes, was further-developed and evaluated for application in climate studies. To evaluate the effects of the added processes on the water budget and soil temperature, simulations are carried out without restart for 2050 days. In doing so, HTSVS was driven by meteorological data routinely measured at Brandis climate station from May 23, 1992 to December 31, 1997. The additions made to HTSVS are to accommodate the effects of water extraction by roots, and soil wetness on soil albedo. A more sophisticated parameterization of infiltration, a soil frost parameterization, and some effects of a snow-pack have been included. HTSVS differs from other LSMs by its consideration of the Dufour- and Ludwig-Soret effects, the diffusion of water vapor within the soil, and a vertically variable distribution of soil type and roots. It has been found that the Dufour- and Ludwig-Soret effects play a notable role on the long-term water budget (Table 3) and soil temperature evolution (e.g., Fig. 7). The diffusion of water vapor within the soil is a prerequisite to include emission of NO_2, and the emission of gases released when permafrost thaws. Especially, in regions of glacially and/or fluvial origin, layered soils exist. Thus, vertically variable soil types may improve climate simulations if global data sets of vertical soil distribution become available. Sensitivity studies show that knowledge on soil parameters and soil heterogeneity may affect the predicted water budget elements (see also Table 3). Based on the results of the simulations with and without root parameterizations and the uncertainty studies on root effects, we have to conclude that the vertical distribution of roots can be important for the predicted water budgets. Therefore, global data sets on the annual course of root distribution for the various vegetation types are required in climate modeling.

Since no data of the radiative forcing were available, uncertainty studies using various parameterizations of long-wave downward radiation had been performed. These studies confirm the results of Slater et al (1998) that the parameterization of long-wave downward radiation may strongly affect the model results. Thus, special efforts should be spent on parameterizing this quantity in climate modeling.

Simulations alternatively performed with and without consideration of snow and soil frost emphasize the great impact of insulating by snow-pack and freezing of soil on soil water budget. Soil frost, and/or snow influence soil temperature even long after their occurrence (cf. Figs. 8 and 9). The results yielded from the simulations with and without frost parameterization show that including the effect of frost improves the prediction of soil temperatures. Snow density and depth strongly affect soil temperature, soil freezing and the water supply to the atmosphere, but hardly influence deep soil water fluxes like recharge in the long-term sum (cf. Table 3). Thus, we may expect that under the consideration of snow metamorphism a time varying snow density and retention of melt-water in the snow-pack may influence soil volumetric water content and recharge more strongly than found here.

Acknowledgements

We would like to express our thanks to J. Rehnert and F. Weisse for their help in data exchange. Thanks also to H. Wanner, J. E. Walsh and the anonymous reviewers for helpful discussion and fruitful comments. Our thanks are also to K. E. Erdmann, and C. T. Qu. We thank BMBF, DFG and NSF for financial support under contracts 01LA98394, 01 LD 00036, Mo770/2-1, and OPP/0002239, respectively.

References

Baker JM, Davis KJ, Liknes GC (1999) Surface energy and water balance and boundary-layer development during snowmelt. J Geophys Res 104D: 19611–19621

Bolz HM, Falkenberg G (1949) Neubestimmung der Konstanten der Angströmschen Strahlungsformel. Z Meteorol 3: 97–100

Boone A, Masson A, Meyers T, Noilhan J (2000) The influence of soil freezing on simulations by a soil-vegetation-atmosphere scheme. J Appl Meteor 39: 1544–1569

Cherkauer KA, Lettenmaier DP (1999) Hydrologic effects of frozen soils in the upper Mississippi river basin. J Geophys Res 104D: 19611–19621

Cowan IR (1965) Transport of water in soil-plant-atmosphere system. J Appl Ecol 2: 221–239

Clapp R, Hornberger G (1978) Empirical equations for some soil hydraulic properties. Water Resour Res 14: 601–604

Croley TE, II (1989) Verifiable evaporation modeling on the Laurentian Great Lakes. Water Resour Res 25: 781–792

Deardorff JW (1978) Efficient prediction of ground surface temperature and moisture, with inclusion of a layer of vegetation. J Geophys Res 84C: 1889–1903

de Groot SR (1951) Thermodynamics of irreversible processes. New York: Interscience Publishers, 242 pp

de Vries DA (1958) Simultaneous transfer of heat and moisture in porous media. T Am Geophys Union 39: 909–916

Dingman SL (1994) Physical hydrology. New York Oxford Singapore Sydney: Macmillan, 575 pp

Eppel DP, Kapitza H, Claussen M, Jacob D, Koch W, Levkov L, Mengelkamp H-T, Werrmann N (1995) The non-hydrostatic mesoscale model GESIMA. Part II: Parameterizations and applications. Contrib Atmos Phys 68: 15–41

Federer CA (1979) A soil-plant-atmosphere model for transpiration and availability of soil water. Water Resour Res 15: 555–562

Flerchinger GN, Hanson CL (1989) Modeling soil freezing and thawing on a rangeland watershed. Trans ASAE 32: 1551–1554

Fuchs M, Campbell GS, Papendick RI (1978) An analysis of sensible and latent heat flow in partially frozen unsaturated soil. Soil Sci Soc Am J 42: 379–385

Fröhlich K, Mölders N (2002) Investigations on the impact of explicitly predicted snow metamorphism on the microclimate simulated by a meso-β/γ-scale non-hydrostatic model. Atmos Res 62: 71–109

Gardner WR (1960) Dynamic aspects of water availability to plants. Soil Sci 89: 63–73

Gardner WR, Ehlig CF (1963) The influence of soil water on transpiration by plants. J Geophys Res 68: 5719–5724

Haferkorn U (2001) Größen des Wasserhaushaltes verschiedener Böden unter landwirtschaftlicher Nutzung im klimatischen Grenzraumes des Mitteldeutschen Trockengebietes. PhD thesis Univ. Göttingen (available from the author or http://webdoc.sub.gwdg.de/diss/2001/haferkorn/index.html)

Hicks BB, Baldocchi DD, Meyers T-P, Hosker RP Jr, Matt RP (1987) A pre-liminary multiple resistance routine for deriving dry deposition velocities from measured quantities. Water, Air, and Soil Pollut 36: 311–330

Idso SD, Jackson RD (1969) Thermal radiation from the atmosphere. J Geophys Res 74: 5397–5403

Jackson RB, Canadell J, Ehleringer JR, Mooney HA, Sala OE, Schulze ED (1996) A global analysis of root distributions for terrestrial biomes. Oecologia 108: 389–411

Jarvis PG (1976) The interpretation of the variations in leaf water potential and stomal conductance found in canopies in the field. Phil Trans R Soc Lond B 273: 593–610

Keese U, Nitsche C, Knappe S, Waldschmidt U (1997) Vergleichende bodenphysikalische Untersuchungen zwischen Lysimetern und ihren Herkunftsflächen am Beispiel von drei typischen Böden Mitteldeutschlands unter landwirtschaftlicher Nutzung. I. Mitteilung. Ermittlung bodenphysikalischer Kenngrößen. Arch Acker- Pfl Boden 41: 209–231

Kramm G (1989) The estimation of surface layer parameters from wind velocity, temperature and humidity profiles by least squares methods. Bound Lay Meteorol 48: 315–327

Kramm G (1995) Zum Austausch von Ozon und reaktiven Stickstoffverbindungen zwischen Atmosphäre und Biosphäre. Frankfurt: Maraun-Verlag, p 268

Kramm G, Beier N, Foken T, Müller H, Schröder P, Seiler W (1996) A SVAT-scheme for NO, NO_2, and O_3 – model description. Meteorol Atmos Phys 61: 89–106

Marshall JT, Holmes JW, Rose CW (1996) Soil Physics. Cambridge University Press, 453 pp

Martin P (1990) Forst succesion and climatic change: coupling land-surface processes and ecological dynamics. PhD Thesis NCAR/CT-131 (available from NCAR, P.O. Box 3000, Boulder, CO 80307, USA)

McCumber MC, Pielke RA (1981) Simulation of the effects of surface fluxes of heat and moisture in a mesoscale model, I soil layer. J Geophys Res 86: 9929–9938

Mölders N (1999) Einfache und akkumulierte Landnutzungsänderungen und ihre Auswirkungen auf Evapotranspiration, Wolken- und Niederschlagsbildung. Wiss Mitt Univ Leipzig, Habil-Schrift, 15: 206 pp (available from the author or by order from bookstores ISBN3-9806117-4-4)

Mölders N (2000) HTSVS – A new land-surface scheme for MM5. In: The tenth PSU/NCAR Mesoscale model users' workshop, 33–35 (available from NCAR, P.O. Box 3000, Boulder, CO 80307, USA or http://www.mmm.ucar.edu/mm5/mm5-home.html)

Oke TR (1978) Boundary layer climates. London New York: Routledge, 435 pp

Paulson CA (1970) The mathematical representation of wind speed and temperature profiles in the unstable atmospheric surface layer. J Appl Meteor 9: 857–861

Pielke RA (1984) Mesoscale meteorological modelling. London: Academic Press

Philip JR (1957) Evaporation, and moisture and heat fields in the soil. J Meteor 14: 354–366

Philip JR, de Vries DA (1957) Moisture in porous materials under temperature gradients. Trans Am Geophys Soc 18: 222–232

Prigogine I (1961) Introduction to thermodynamics of irreversible processes. New York London: Interscience Publishers, 119 pp

Robinson DA, Serreze MC, Barry RG, Scharfen G, Kukla G (1992) Large scale patterns and variability of snowmelt and parameterized surface albedo in the Arctic Basin. J Climate 5: 1109–1119

Rosenberg NJ, McKenney MS, Martin P (1990) Evapotranspiration in a greenhouse-warmed world: A review and a simulation. Agricultural Forest Meteorol 47: 303–320

Schmidt B (1990) Derivation of an explicit equation for infiltration on the basis of the Mein-Larson model. Hydrol Sci J 35: 197–208

Schlosser CA, Slater AG, Robock A, Pitman AJ, Vinnikov KY, Henderson-Sellers A, Speranskaya NA, Mitchell K, the PILPS2(d) Contributors (2000) Simulations of a boreal grassland hydrology at Valdai, Russia: PILPS phase 2(d). Mon Wea Rev 128: 301–321

Sellers PJ, Mintz Y, Sud YC, Dalcher A (1986) A simple biosphere model (SIB) for use within general circulation models. J Appl Meteor 43: 505–531

Slater AG, Pitman AJ, Desborough CE (1998) Simulation of freeze-thaw cycles in a general circulation model land surface scheme. J Geophys Res 103D: 11303–11312

Wilson MF, Henderson-Sellers A, Dickinson RE, Kennedy PJ (1986) Sensitivity of the biosphere-atmosphere transfer scheme (BATS) to the inclusion of variable soil characteristics. J Clim Appl Met 26: 341–362

Authors' addresses: N. Mölders (E-mail: molders@gi.alaska.edu) and G. Kramm (E-mail: kramm@gi.alaska.edu), Geophysical Institute, University of Alaska Fairbanks, 903 Koyukuk Drive, Fairbanks, AK 99775-7320, USA; U. Haferkorn, Staatliche Umweltbetriebsgesellschaft, Kleinsteinberger-Str. 13, 04821 Brandis, Germany; J. Döring, Universität Halle-Wittenberg, Institut für Agrarökonomie und Agrarraumgestaltung, Adam-Kuckhoff-Straße 15, 06108 Halle/Saale, Germany